European Conference on Computational Fluid Dynamics
ECCOMAS CFD 2006
P. Wesseling, E. Oñate and J. Périaux (Eds)

LARGE EDDY SIMULATION FOR TURBULENT COMBUSTION IN A CYLINDRICAL COMBUSTOR

Sreebash C. Paul*, Manosh C. Paul† and William P. Jones‡

*,†Department of Mechanical Engineering, University of Glasgow, Glasgow G12 8QQ, UK
e-mail: m.paul@mech.gla.ac.uk
web page: http://www.mech.gla.ac.uk/
‡Department of Mechanical Engineering, Imperial College London, Exhibition Road, London SW7 2AZ, UK
e-mail: w.jones@imperial.ac.uk

Key words: Large Eddy Simulation, Turbulent Flow, Combustion, Beta Probability Density Function, Subgrid Scale Stress

Abstract. *In this work we investigate turbulent non-premixed combustion, including species concentrations and temperature, in a model of 3D cylindrical combustor. Gaseous propane (C_3H_8) and preheated air with temperature of 773K are injected through the combustor inlet. A Large Eddy Simulation (LES) technique is applied to solve the governing equations of motion while the filtered values of species mass fraction, temperature and density, which are functions of the mixture fraction, are determined by integration over a beta Probability Density Function (β-PDF). In LES a spatial filter is used to the governing equations to separate the large scale eddies from the small scale eddies. The large scale eddies which carry most of the turbulent energy are resolved explicitly while the small scale eddies are modelled. The computational results are compared with those of the experimental investigation where a good agreement is achieved.*

1 INTRODUCTION

Turbulent combustion occurs in nature and most engineering applications. Understanding of turbulent combustion process is essential for efficient design of many engineering devices such as gas turbines, internal combustions (IC) engines, furnaces etc. Moreover, the number of combustion system used in transformation and transportation industries is rapidly growing and as a result a huge amount of combustion products such as NO_x, CO and unburned hydrocarbons are produced everyday, which are harmful to human heath and a great threat to the global environment. The accurate control and prediction of turbulent flames and an increment of the performance of combustion efficiency, therefore, appear to be a hot and essential topic in engineering.

Combustion remains one of the most complicated phenomena to describe and simulate using numerical tools, mainly because of a practical combustion process is usually associ-

ated with the turbulent flows. The multi-scale character of turbulence makes simulation of such flows a difficult task. In order to account for the full nonlinear multi-scale effect of turbulence in a combustion process, the governing equations must be solved resolving the micro-scale, known as *Kolmogrov scale*, eddies. However, to date this is not a possible task for flows on that technical scale. Thus, depending on the scale of interest, different techniques with different modelling approaches exist in the literature. Large Eddy Simulation (LES) technique is one of them and has recently been shown to be a promising approach for computation of turbulent flows, because of its clear means of overcoming some of the deficiencies which appear in other available approaches such as Reynolds Averaged Navier Stokes (RANS) and Direct Numerical Simulation (DNS) which are restricted to low Reynolds number flows. The chemical reactions that control combustion, however, occur at the smallest scales of the flow and can almost never be fully resolved. As such, modelling approaches are needed in order to predict accurately the chemical behaviour of reacting flows.

In the RANS technique, the governing equations of motion are averaged first with time, which produces unknown stresses, named as Reynolds stresses since the early work done by Reynolds[1], which are modelled. But in LES technique, a filtering approach is usually used to the governing equations in order to filter out the subgrid scale (sgs) motions from the large scale. The filtering is typically taken over the control volume of a numerical simulation with a suitably defined filter function.

Furthermore, a considerable research has been carried out by Smagorinsky[2] and Lilly[3] on an assumption made for the SGS Reynolds stresses. Their ideas were further developed by Deardorff[4] in the area of engineering applications, who simulated the plane Poiseuille flow (channel flow). Since then, LES has been developed and applied to a number of increasingly complex problems by a large number of researchers, such as LES of turbulent confined coannular jets by Akselvoll and Moin[5], LES of a plane jet in a cross-flow by Jones and Wille[6], and LES of a round jet in a crossflow by Yuan *et al*[7]. Number of recent papers have also demonstrated the power of LES method to the flows of turbulent combustion, such as a LES scheme for turbulent reacting flows by Gao and O'Brien[8], LES of a nonpremixed reacting jet by DesJardin and Frankel[9], LES of a turbulent nonpremixed flame by Branley and Jones [10], and LES of a model gas turbine combustor by di Mare *et al*[11].

In this study we investigate turbulent non-premixed combustion, including species concentrations and temperature, in a model cylindrical combustor using LES. Gaseous propane (C_3H_8) is injected through a circular nozzle of an internal diameter of $2mm$ at the centre of the combustor inlet while the preheated air with an averaged velocity of $0.96ms^{-1}$ and temperature of $773K$ is supplied through the circular inlet of $115mm$ internal diameter into the $1m$ long combustion chamber. The overall equivalence ratio is 1.67 so that burning occurs in a fuel-rich nonpremixed combustion mode. The average fuel velocity of $30ms^{-1}$ at the inlet corresponds to a Reynolds number of $13,000$ is used in the computation. A schematic of the cylindrical combustor with computational domain

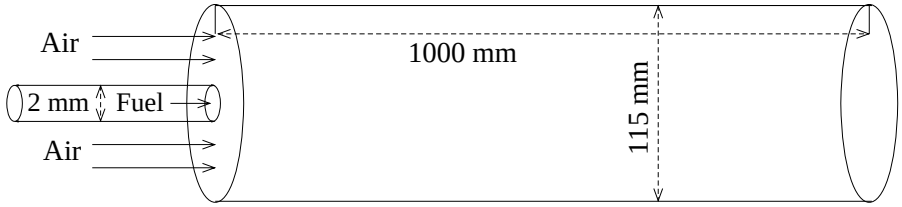

Figure 1: A schematic of the cylindrical combustor with computational domain.

is shown in Figure 1. The present computational results are compared with those of the experimental investigation performed by Nishida and Mukohara[12].

2 GOVERNING EQUATIONS

In large eddy simulation, the spatial filtering operation is used to separate the large scale (resolved scale) flow field from the small scale (sub-grid scale). If $f(x_j, t)$ is a generic instantaneous variable at a location, $x_j = (x, y, z)$, the corresponding filtered (resolved) variable, known as resolvable component of $f(x_j, t)$, denoted by $\bar{f}(x_j, t)$, is defined as the convolution of $f(x_j, t)$ with a filter function G by Leonard[13], according to

$$\bar{f}(x_j, t) = \int_D f(x'_j, t) G(x_j - x'_j, \Delta(x_j)) dx'_j, \tag{1}$$

where D is the entire domain; $\Delta(x_j) = (\Delta x \Delta y \Delta z)^{1/3}$ is the filter width which is generally the mesh size in LES; and G is the suitably defined filter function which must satisfy the normalization condition,

$$\int_D G(x_j - x'_j, \Delta(x_j)) dx'_j = 1. \tag{2}$$

It is important to note that this filter function determines the size and structure of the small eddies. Various distributions of the filter function are available in the literature, for example, see Leonard[13], Germano[14], and Ghosal and Moin[15]. In our simulation we have used the "top hat" filter suggested by Germano[14] as

$$G[x_j - x'_j, \Delta(x_j)] = \begin{cases} \frac{1}{\Delta(x_j)} & \text{if} \quad |x_j - x'_j| \leq \frac{\Delta(x_j)}{2} \\ 0 & \text{otherwise} \end{cases} \tag{3}$$

For the flow with large density variations, like in combustion, it is essential to introduce another filtering approach, namely the Favre-Filter or Favre average (also known as the density weighted filter) by Favre[16]. In the Favre averaging all fluid mechanical quantities except the pressure are mass averaged. The Favre-Filter function is denoted by $\tilde{f}$ and defined as

$$\tilde{f} = \frac{\overline{\rho f}}{\bar{\rho}}. \tag{4}$$

This Favre-Filtering approach has been used extensively in LES studies of compressible turbulence[17,18] and reacting flows[10,11,19,20].

Employing the Favre-Filtered function to the continuity, momentum conservation and mixture fraction equations gives:

$$\frac{\partial \bar{\rho}}{\partial t} + \frac{\partial(\bar{\rho}\tilde{u}_j)}{\partial x_j} = 0, \tag{5}$$

$$\frac{\partial(\bar{\rho}\tilde{u}_i)}{\partial t} + \frac{\partial(\bar{\rho}\widetilde{u_i u_j})}{\partial x_j} = -\frac{\partial \bar{p}}{\partial x_i} + \frac{\partial}{\partial x_j}\left[2\mu\bar{S}_{ij} - \frac{2}{3}\mu\bar{S}_{kk}\delta_{ij}\right], \tag{6}$$

$$\frac{\partial \bar{\rho}\tilde{\xi}}{\partial t} + \frac{\partial \bar{\rho}\widetilde{u_j \xi}}{\partial x_j} = \frac{\partial}{\partial x_j}\left(\Gamma\frac{\partial \tilde{\xi}}{\partial x_j}\right), \tag{7}$$

where t is time; x_j is any of the three coordinate directions; u_j is any of the three velocity components; p is the pressure; ρ is the density, which, in reacting flows, varies due to the heat release from the chemical reaction and on the chemical composition of the fluid. μ is the molecular viscosity, $S_{ij} = \frac{1}{2}(\frac{\partial u_i}{\partial x_j} + \frac{\partial u_j}{\partial x_i})$ is the strain rate, δ_{ij} is the kronecker delta, ξ is the conserved scalar or mixture fraction and $\Gamma = \frac{\mu}{Pr} = \frac{\mu}{Sc}$ is the diffusion coefficient.

3 SUBGRID-SCALE MODELLING

An application of the density weighted filter to the nonlinear convective terms in the system of governing equations introduces the unknown terms $\bar{\rho}\widetilde{u_i u_j}$ and $\bar{\rho}\widetilde{u_j \xi}$ in equations (6,7), leaving the equations (6,7) unclosed. These unknown terms are defined by Germano [21] as

$$\bar{\rho}\widetilde{u_i u_j} = \bar{\rho}\tilde{u}_i\tilde{u}_j + \tau_{ij} \tag{8}$$

and

$$\bar{\rho}\widetilde{u_j \xi} = \tilde{u}_j\tilde{\xi} + J_j^{sgs} \tag{9}$$

where τ_{ij} and J_j^{sgs} are unknown and referred to as subgrid scale stresses and subgrid scale scaler fluxes respectively. These unknowns must be modelled.

The most famous and still widely used model for the subgrid scale stress is that of the Smagorinsky model[2]. The model is based on eddy viscosity assumption and of the form of

$$\tau_{ij} - \frac{1}{3}\delta_{ij}\tau_{kk} = -2\nu_{sgs}\bar{S}_{ij}, \tag{10}$$

where the subgrid kinetic eddy viscosity, ν_{sgs}, related to the subgrid eddy viscosity, μ_{sgs}, as $\nu_{sgs} = \frac{\mu_{sgs}}{\rho}$, obtained by assuming that the turbulent dissipation is in equilibrium with the turbulent energy production. This yields an expression of

$$\nu_{sgs} = \bar{\rho}(C_s\Delta)^2|\bar{S}|, \tag{11}$$

where C_S is the Smagorinsky constant and $|\bar{S}| = \sqrt{2\bar{S}_{ij}\bar{S}_{ij}}$ is the magnitude of the large scale strain rate tensor, $\bar{S}_{ij}$. The value of the Smagorinsky constant, C_s, is to be assigned in the computation, which takes the typical value of around 0.1.

Commonly used model for the subgrid scale scalar flux by Schmidt and Schumann [22] is of the form

$$J_j^{sgs} = -\bar{\rho}\Gamma_{sgs}\frac{\partial\tilde{\xi}}{\partial x_j} = -\frac{\bar{\rho}\nu_{sgs}}{Pr_{sgs}}\frac{\partial\tilde{\xi}}{\partial x_j}, \tag{12}$$

where Pr_{sgs} is the subgrid scale Prandtl/Schmidt number which takes a value of 0.7 in our computation.

4 β - PROBABILITY DENSITY FUNCTION (β-PDF) MODEL IN LES

Once the density weighted mixture fraction, $\tilde{\xi}$, has been obtained from its transport equation (7), the filtered density and density weighted thermochemical variables ($\tilde{\phi}_i$) are obtained respectively from

$$\bar{\rho}(\tilde{\xi}) = \left(\int_0^1 \frac{\tilde{P}(\xi,\tilde{\xi})}{\rho(\xi)}d\xi\right)^{-1} \tag{13}$$

and

$$\tilde{\phi}(\tilde{\xi}) = \int_0^1 \phi(\xi)\tilde{P}(\xi,\tilde{\xi})d\xi, \tag{14}$$

where $\tilde{P}(\xi,\tilde{\xi})$ is the density weighted i.e. Favre-filtered β - PDF, which satisfies the normalization condition,

$$\int_0^1 \tilde{P}(\xi,\tilde{\xi})d\xi = 1, \tag{15}$$

and is defined by

$$\tilde{P}(\xi,\tilde{\xi}) = \frac{\xi^{r-1}(1-\xi)^{s-1}}{\beta(r,s)}, \tag{16}$$

where

$$r = \tilde{\xi}\left(\frac{\tilde{\xi}(1-\tilde{\xi})}{\widetilde{\xi''^2_{sgs}}} - 1\right) \quad , \quad s = \frac{1-\tilde{\xi}}{\tilde{\xi}}r \tag{17}$$

and

$$\beta(r,s) = \int_0^1 \xi^{r-1}(1-\xi)^{s-1}d\xi \tag{18}$$

is the beta function.

For the subgrid scalar variance of the mixture fraction, $\widetilde{\xi''^2_{sgs}}$, we have employed the widely used gradient model proposed by Pierce and Moin[23] as

$$\widetilde{\xi''^2_{sgs}} = C_\xi\Delta^2\left|\frac{\partial\tilde{\xi}}{\partial x_j}\frac{\partial\tilde{\xi}}{\partial x_j}\right|, \tag{19}$$

where C_ξ is the model parameter assigned the value of 0.1 as Branley and Jones[10].

5 INTEGRATING THE SUBGRID β-PDF

The relationship between the thermochemical variables and the mixture fraction are expressed as a polynomial of degree n in the conserved scalar as

$$\phi(\xi) = \sum_{m=0}^{n} a_m \xi^m. \tag{20}$$

Substituting the polynomial relation (20) and the $\beta - pdf$ (16) into equation (14), the Favre-Filtered scalar quantities can now be rewritten as

$$\tilde{\phi}(\tilde{\xi}) = \int_0^1 \sum_{m=0}^{n} a_m \xi^m \frac{\xi^{r-1} - (1-\xi)^{s-1}}{\beta(r,s)} d\xi. \tag{21}$$

Making use of the beta function given in (18) and the Gamma(Γ) function defined as

$$\Gamma(r) = \int_0^\infty e^{-x} x^{r-1} dx, \tag{22}$$

with the relationships between β and Γ functions as,

$$\beta(r,s) = \frac{\Gamma(r)\Gamma(s)}{\Gamma(r+s)}, \tag{23}$$

the filtered scalar quantities are finally computed through the following series,

$$\tilde{\phi}(\tilde{\xi}) = \sum_{m=0}^{n} \frac{a_m (r+m-1)!(r+s-1)!}{(r+s+m-1)!(r-1)!}, \tag{24}$$

where the coefficients a_0, a_1, ..., a_n are obtained from the polynomial fitting on the flamelet data against the mixture fraction shown in Figure 2.

6 NUMERICAL PROCEDURE

A curvilinear body fitted coordinate system is employed for the present simulation consisting of a total of $1,383,840$ cells with grid nodes of $93 \times 93 \times 160$ in the x, y, z directions respectively. A schematic of the computational geometry with domain has been shown in Figure 1. A non-uniform mesh is generated inside the combustion chamber. At the centre of the combustor inlet, where the fuel is injected through the circular nozzle with relatively higher speed than air through the cylinder, it was required to use a very fine mesh in the fuel injection area so that the steep gradients appear in this area are better resolved. The meshlines are contracted at the centre and near the inlet of the combustor, and they are expanded smoothly in all three directions outwards from the centreline and inlet.

The numerical solution procedure employed here is based on the finite volume approach where the Favre-filtered Navier-Stokes and the mixture fraction transport equations are

integrated over the mesh control volume. The in-house developed LES-BOFFIN (Boundary Fitted Flow Integrator) code has been used to solve the governing equations, which is based on a fully implicit low-Mach number formulation and is second order accurate in both space and time. The BOFFIN code has extenssively been applied previously by many authors in the LES of reacting and non-reacting turbulent flows, for examples, see LES of a gas turbine combustor[11], of a turbulent non-premixed flame[10], and of turbulent flow past a swept fence[24]. For a full details of the numerical method used in the BOFFIN, the readers are referred to those published papers.

The spatial derivatives in equations (1,2) are discretised using the standard second order accurate central difference scheme, except for the convective terms in the momentum equations (2) for which an energy conserving discretisation scheme is used. The central differencing scheme for discretising the convection terms in the mixture fraction equation (3) may result in overshoots and undershoots in the mixture fraction when the cell peclet numbers are greater than 2. However, the mixture fraction must remain bounded between its maximum and minimum values, to avoid any unphysical results of the density, temperature and species concentrations occur in the computation. In order to avoide this, a Total Variation Diminishing (TVD) scheme of Sweby[25] has been used to discretise the convection terms in the mixture fraction transport equation, and no unphysical values of the mixture fraction are computed in the simulation. Time derivatives are approximated by a three point backward difference scheme with variable time step.

To determine the pressure, we have used a two step second-order time-accurate approximate factorisation method to ensure mass conservation. Pressure and velocity terms are linked according to a SIMPLE type algorithm where a colocated arrangement is used to store results at the cell centres. Rhie and Chow[26] pressure smoothing technique is also used to prevent even-odd node uncoupling of the pressure and velocity fields. The system of algebraic equations resulting from the discretisation has been solved by using Matrix pre-conditioned conjugate gradient methods, Bi-CGSTAB[27] for the velocity and scalar equations and ICCG (1,1,1)[28,29] for the pressure.

In the simulation the instantaneous inflow boundary conditions for the velocity component along the horizontal direction is used to be an average value of $30ms^{-1}$ at the fuel nozzle and $0.96ms^{-1}$ for the air flow, but for the velocities at the radial directions are kept at zero. The mixture fraction at the inlet is defined as

$$\xi = \begin{cases} 1 & \text{in the fuel stream} \\ 0 & \text{in the air stream.} \end{cases} \tag{25}$$

At the outlet boundary, a zero-gradient boundary condition (also referred to *reflective*) has been used, this condition was sufficient to minimise the effects of the outlet boundary on the solutions. A thin viscous sub-layer grows on the wall of the combustor, a fine mesh is also required in the simulation to resolve that layer, which turns to be a very expensive computation. To overcome this difficulty, an instantaneous log-law wall condition is employed for the surfaces of the combustor.

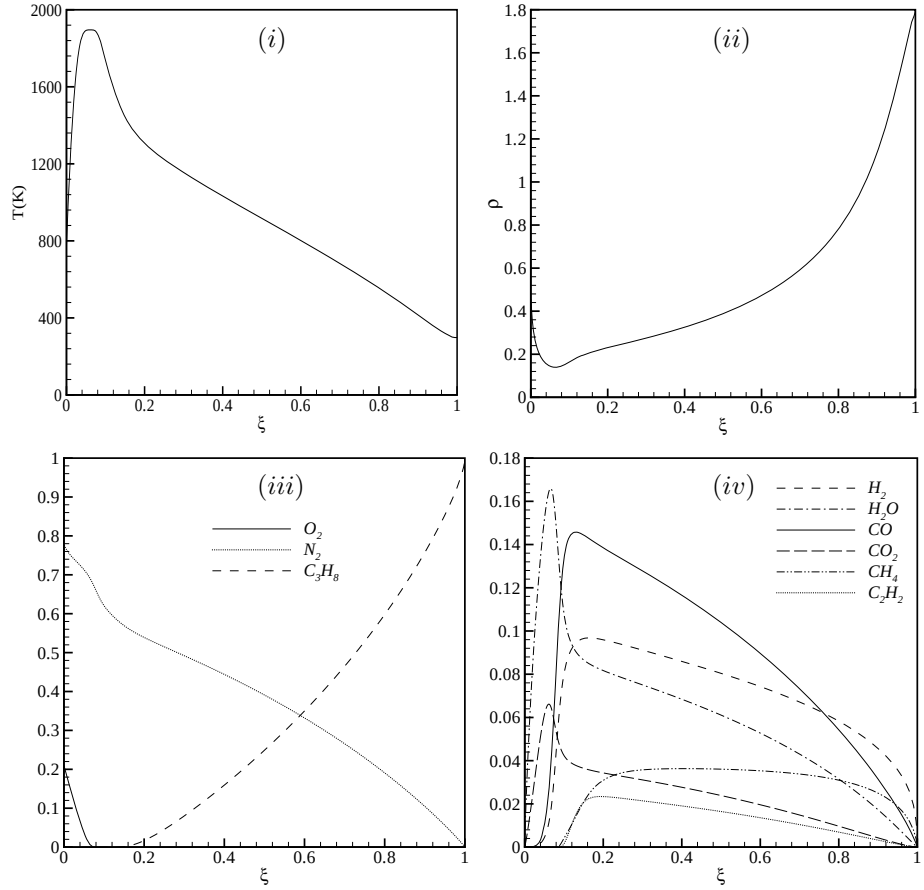

Figure 2: Laminer flamelet calculation (strain rate = $15s^{-1}$): Dependence of (i) temperature, (ii) density and (iii)-(iv) species mole fraction (ϕ_i) on the mixture fraction, ξ.

7 RESULTS AND DISCUSSIONS

In this section we now present some of the computational results obtained after $100,000$ time iterations, which is at the real clock time of $t = 0.2737sec$. As mentioned in the previous section that a variable time step is used in the computations to ensure that the maximum Courant number ($\tilde{u}_j \frac{dt}{dx_j}$) lies between 0.1 and 0.2, this was essential to prevent the simulation not becoming unstable as the radial velocities of the flame increase with time[30]. The average time step, dt, used in the computation is at the order of 10^{-6}.

Laminar flamelet calculation for the dependence of temperature, density and species mole fraction on the mixture fraction (ξ) used in the combustion model are given in Figure 2. The flamelet was generated with a strain rate of $15s^{-1}$ and the boundary conditions were taken to adjust with the experimental preheated conditions for the air.

In the first frame of figure 2 the temperature variation against the mixture fraction is plotted and the corresponding density variation is shown in frame (ii). When $\xi = 0$ the mixture fraction consists of air stream only, as described in the boundary condition

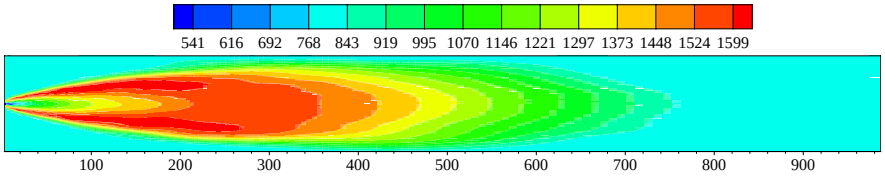

Figure 3: Mean temperature, $< \tilde{T} >$, plot on the horizontal midplane of the combustor.

in the previous section, the mean temperature of $T = 773K$ represents the preheated air temperature. While at $\xi = 1$, where the mixture fraction consists of fuel stream only, $T = 298K$ represents the mean fuel (propane) temperature. At the stoichiometric level of the mixture fraction (ξ_{stoich}), which is at about $\xi_{stoich} = 0.06$, the oxygen and fuel stream curves meet together and react, and a maximum temperature of $T = 1896K$ is achieved, see frame (i). The corresponding density of the mixture at the stoichiometric level has its minimum value as expected, see frame (ii). It is worth to mention here that for an equilibrium combustion model one could achieve a linear relationship for the oxygen, fuel and reactant products against the mixture fraction, which is unlikely to the flamelet approach to a non-premixed combustion model where the linear relations no longer hold, as shown in all frames of figure 2.

In frame (iv) the mole fraction of the combustion products, taken into account in the flamlet calculation, is also shown. It is interesting to note that at ξ_{stoich} mole fractions of CO_2 and H_2O have their maximum value but for other species the peak levels are moved into the right direction along ξ at the region of $\xi_{stoich} < \xi < 1$ where a fuel-rich condition is prevailed. A polynomial of degree $n = 20$, as described in section 5, was fitted on each flamelet data set, shown in figure 2, to achieve the power coefficients, a_m, of the polynomial described in equation (24). These power coefficient data were used as an input in the computation. Once the instantaneous results of the mixture fraction and the variance of the mixture fraction were computed, using the power coefficient data, we have finally achieved the filtered quantities of the flame temperature, density, and species from the relation (24).

The mean values of the flame temperature, $< \tilde{T} >$, on the horizontal midplane of the combustion chamber is shown in figure 3. The contour levels show that at the centre of the combustor the flame temperature increases along the axial direction, and before it reaches to the half way through the flame temperature drops gradually and eventually attains the same as the air temperature at the downstream. The former issue can clearly be seen in figure 4 when the radial distance is zero i.e. at the centre of the combustor, where the predicted as well as the measured temperature increases as the axial distance increases from frames (a) to (d).

In figure 4 the computationally predicted mean, $< \tilde{T} >$, and Favre-averaged, $\tilde{T}$, temperature results are compared against the experimental measurement done by Nishida and Mukohara[12]. The results in figure 4 are taken along the radial direction at four different

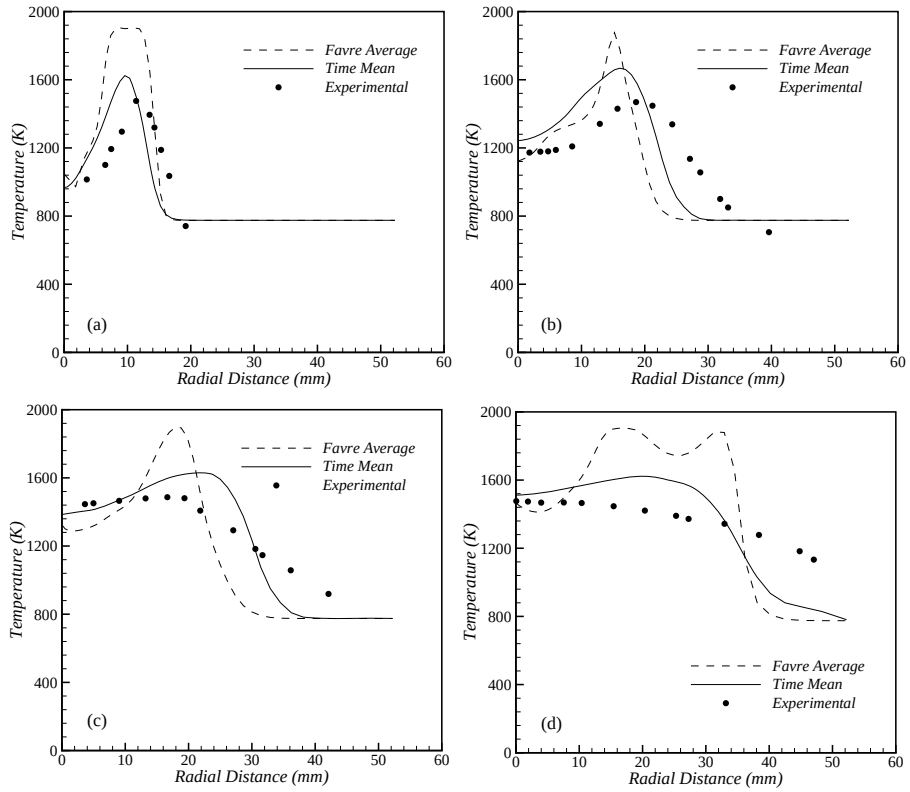

Figure 4: Comparisons of the mean temperature ($< \tilde{T} >$) and Favre average temperature ($\tilde{T}$) against experimental data along the radial direction at different cross-sectional positions: (a) 100mm, (b) 200mm, (c) 300mm and (d) 400mm axial distance from the inlet.

cross-sectional positions, (a) 100mm, (b) 200mm, (c) 300mm and (d) 400mm. Near the inlet the peak flame temperature is recorded at the radial distance of about $10mm$ (see frame (a)), where a good agreement against the experiment has achieved. As we move along the axial direction, the following frames (b)-(d) show how the flame spreads along the radial direction of the combustor, which is also quite clear from the contour plot of $< \tilde{T} >$ shown in figure 3. The experimental investigation also shows the same trend here. The important significance of these phenomenon will be looked at figure 5 where the corresponding mixture fractions are presented.

In figure 5 radial profiles of the mean and instantaneous results of the mixture fraction are plotted along the radial direction. The computational data are taken at the same axial directions as we did for the flame temperatures, shown in the previous figure. The black circle in each frame indicates where the stoichiometric level of the mixture fraction, already described in the flamelet profiles shown in figure 2, occurs in the computation. At frame (a) the stoichiometric mixture fraction is recorded at about the radial distance of 10mm, which again corresponds the maximum flame temperature we achieved at the same location, shown in frame (a) of figure 4. At frames (b)-(d) we can also see that

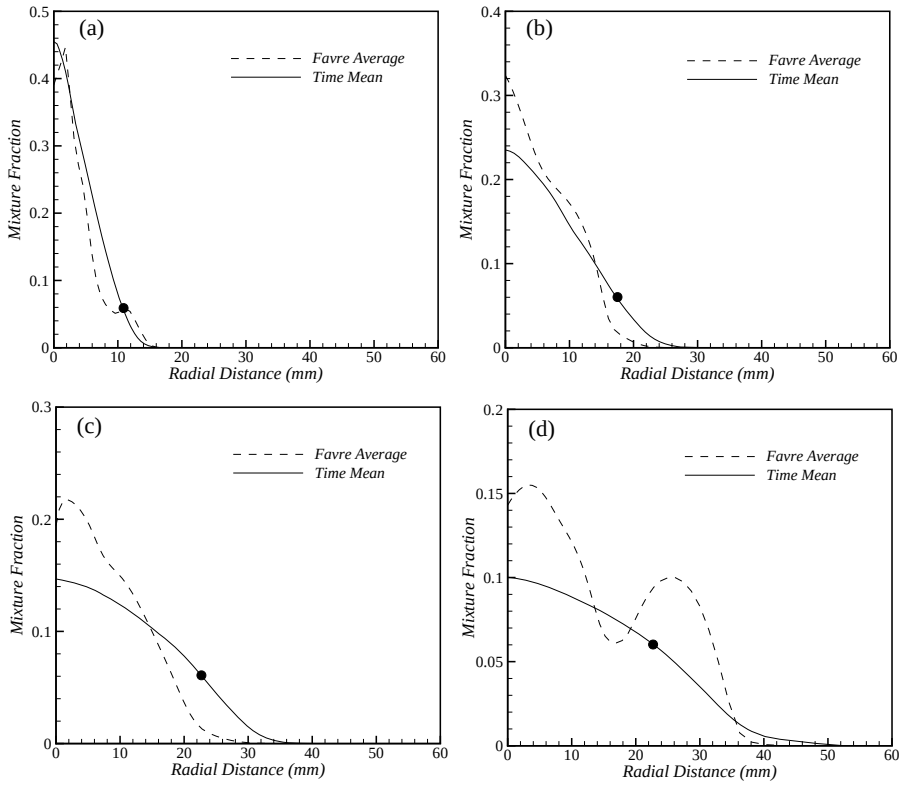

Figure 5: Radial profiles of the mixture fraction at various axial distances from the inlet; (a) 100mm, (b) 200mm, (c) 300mm and (d) 400mm.

the stoichiometric value of the mixture fraction moves along the radial direction from the centre line, which again coincides with the early predictions of the temperature we have in frames (b)-(d) of figure 4.

Comparing the results of the mixture fraction among all frames in figure 5, it can be seen that it is highest near the inlet, see frame (a); but it decays along the axial direction, see frames (b)-(d). This is very significant given that the boundary condition of the mixture fraction used in the simulation was maximum for the fuel stream at the combustor inlet. The injected fuel through the centre of the combustor inlet reacted with the supplied air and produced the combustion products (shown in figure 6), therefore, the mixture fraction expected to decay along the axial direction as well as the radial direction where the air stream dominates.

In figure 6 comparisons with experiment of the predicted radial profile of mean mole fraction, $\tilde{Y}_i$, along with the Favre-averaged mole fraction of some selected combustion species are given. These results are taken at 100mm axial distance from the inlet and plotted along the radial direction, which correspond to the temperature and mixture fraction results shown in frame (a) of figures 4-5. In the first three frames of figure 6, it can be seen that the mole fraction of the three reactants, $\tilde{Y}_{N_2}$, $\tilde{Y}_{O_2}$ and $\tilde{Y}_{C_3H_8}$ are well

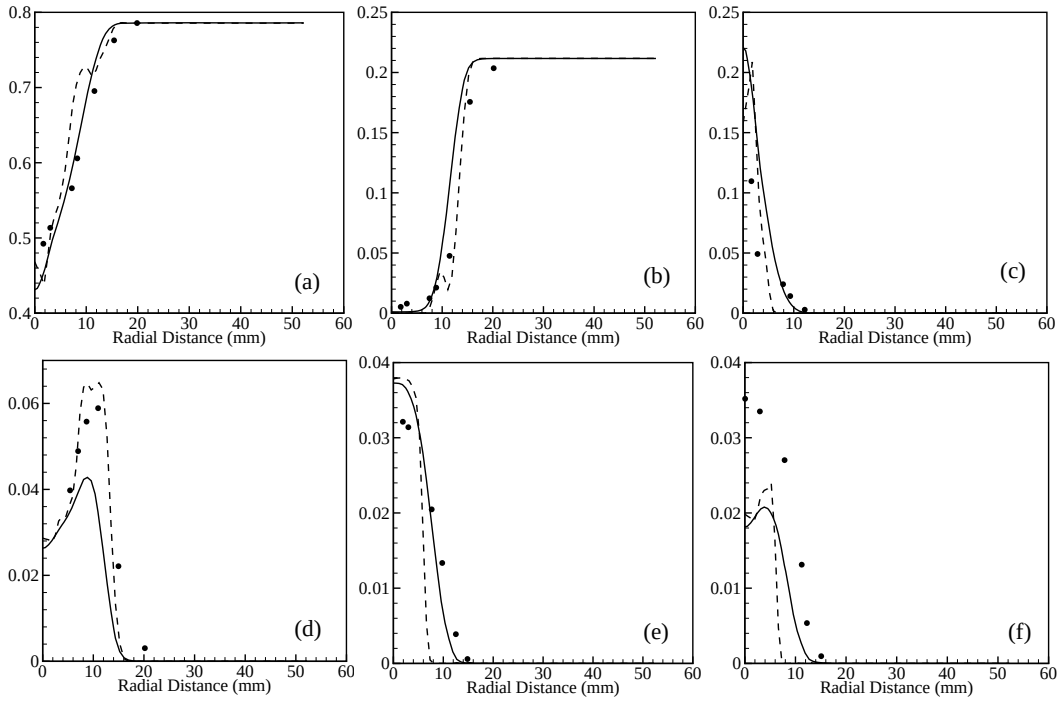

Figure 6: Radial mole fraction at 100mm axial distance from inlet position: (a) $\tilde{Y}_{N_2}$, (b) $\tilde{Y}_{O_2}$, (c) $\tilde{Y}_{C_3H_8}$, (d) $\tilde{Y}_{CO_2}$, (e) $\tilde{Y}_{CH_4}$ and (f) $\tilde{Y}_{C_2H_2}$; Solid lines, Time mean; dashed line, Favre averaged; dot, experiment.

predicted against the experiment, whereas the combustion products $\tilde{Y}_{CO_2}$ (see frame (d)) and $\tilde{Y}_{C_2H_2}$ (see frame (f)) slightly over-predicted but $\tilde{Y}_{CH_4}$ (see frame (e)) is well-predicted. In the combustion process some unburned hydrocarbons, such as CH_4 and C_2H_2 formed due to the fact that the burning occurs in a fuel-rich nonpremixed combustion mode with the overall equivalence ratio of 1.67.

In figure 7 we have plotted the instantaneous results of the streamlines at different cross sections along the axial direction of the combustor, in order to show the turbulent flow field and structure inside the combustor chamber. Looking at each frame in this figure, we can conclude immediately how intensive and chaotic of the flow is inside the combustor. Near the inlet a vortex core initially develops at the centre of the combustor as shown in frame (a) for 100mm. But, as we move along the axial direction the frames (b)-(f) show how quickly the central vortex spreads towards the boundary of the cylinder. Multiple vortices with a different strength also generate inside the combustor which then grow, spread, dominant and drive the flow.

8 CONCLUSIONS

Large Eddy Simulation technique has been applied to analyse the turbulent flow and species concentration with temperature during the non-premixed propane/air turbulent combustion process within a cylindrical combustor. The computational results have been

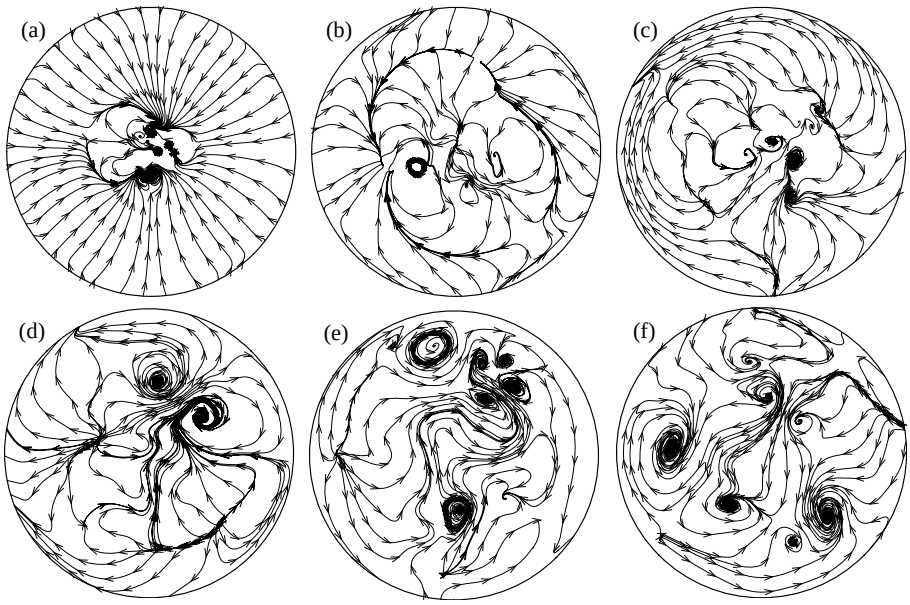

Figure 7: Instanteneous streamlines at different axial distances; (a) 100mm, (b) 200mm, (c) 300mm, (d) 400mm, (e) 500mm, and (b) 600mm

compared with the experimental data obtained by Nishida and Mukohara[12] in the turbulent propane and preheated air combustion, where a good agreement is achieved.

In the present model the combustion occurs in a fuel-rich condition where the overall equivalence ratio of 1.67 is used, which produces some forms of unburned hydrocarbons in the combustion products. One of them is acetylene, C_2H_2, which contributes to the formation and growth of soots (solid carbon particles, solid emissions) in the combustion process. In order to predict the soot formation and growth in the same flame, this work has been extended including two conservative equations, one for the soot mass fraction and another for the soot particle density.

REFERENCES

[1] O. Reynolds. On the dynamical theory of incompressible viscous fluids and the determination of the criterion. *Phil. Trans.* **186 (Series A)**, 123–164, (1895).

[2] J. Smagorinsky. General circulation experiments with the primitive equations I. The basic experiment. *Monthly Weather Review*, **91 (3)**, 99–164, (1963).

[3] D. K. Lilly. The representation of small scale turbulence in numerical simulation experiments. *Proc. IBM Scientific Computing Symposium on Environmental Science*, White Blains, N. Y., 195–210, (1967).

[4] J. W. Deardorff. A numerical study of three dimensional turbulent channel flow at large Reynolds numbers. *Journal of Fluid Mechanics*, **41 (2)**, 453–480, (1970).

[5] K. Akselvoll and P. Moin. Large-eddy simulation of turbulent confined coannular jets. *Journal of Fluid Mechanics*, **315**, 387–411, (1996).

[6] W. P. Jones and M. Wille. Large-eddy simulation of a plane jet in a cross-flow. *Int. J. Heat and Fluid Flow*, **17**, 296–306, (1996).

[7] L. L. Yuan, R. L. Street and J. H. Ferziger. Large-eddy simulation of a round jet in a cross-flow. *Journal of Fluid Mechanics*, **379**, 71–104, (1999).

[8] F. Gao and E. E. O'Brien. A large-eddy simulation scheme for turbulent reacting flows. *Phys. Fluids A*, **5 (6)**, 1282–1284, (1993).

[9] P. E. DesJardin and H. Frankel. Large sddy simulation of a nonpremixed reacting jet: Application and assessment of subgrid-scale combustion models. *Physics of Fluids*, **10 (9)**, 2298–2314, (1998).

[10] N. Branley and W. P. Jones. Large Eddy Simulation of a Turbulent Non-premixed Flame. *Combustion and Flame*, **127**, 1914–1934, (2001).

[11] F. di Mare, W. P. Jones, and K. R. Menzies. Large eddy simulation of a model gas turbine combustor. *Combustion and Flame*, **137**, 278–294, (2004).

[12] O. Nishida and S. Mukohara. Characteristics of soot formation and decomposition in turbulent diffusion flames. *Combustion and Flame*, **47**, 269–279, (1982).

[13] A. Leonard. Energy cascade in large eddy simulations of turbulent flows. *Advances in Geophysics*, **18 (A)**, 237–248, (1974).

[14] M. Germano. Turbulence, the filtering approach. *Journal of Fluid Mechanics*, **238**, 325–336, (1992).

[15] S. Ghosal and P. Moin. The Basic Equation for the Large Eddy Simulation of turbulent flows in Complex Geometry. *Journal of Computational Physics*, **118**, 24–37, (1995).

[16] A. Favre. Statistical equations of turbulent cases in problems of hydrodynamics and continuum mechanics. *Tech. rep., Society of Industrial and Applied Mathematics, Philadelphia*, (1969).

[17] P. Moin, K. Squires, W. Cabot, and S. Lee. A dynamic subgrid-scale model for compressible turbulence and scalar transport. *Physics of Fluids A*, **3 (11)**, 2746–2757, (1991).

[18] G. Erlebacher, M. Y. Hussaini, C. G. Speziale, and T. A. Zang. Towards the large-eddy simulation of compressible turbulent flows. *Journal of Fluid Mechanics*, **238**, 155–185, (1992).

[19] H. Steiner and W. K. Bushe. Large eddy simulation of a turbulent reacting jet with conditional source-term estimation. *Physics of Fluids*, **13 (3)**, 754–769, (2001).

[20] W. K. Bushe and H. Steiner. Conditional moment closure for large eddy simulation of non-premixed turbulent reacting flows. *Physics of Fluids*, **11 (7)**, 453–480, (1970).

[21] M. Germano. A proposal for a redefinition of the turbulent stress in the filtered Navier-Stokes equations. *Physics of Fluids*, **29 (7)**, 2323-2324, (1986).

[22] H. Schimdt and U. Schumann. Coherent structure of the convective boundary layer derived from large-eddy simulations. *journal of Fluid Mechanics*, **200**, 511–562, (1989).

[23] C. D. Pierce and P. Moin. A dynamic model for subgrid-scale variance and dissipation rate of conserved scalar. *Physics of Fluids*, **10 (12)**, 3041–3044, (1998).

[24] L. di Mare and W. P. Jones. LES of turbulent flow past a swept fence. *International Journal of Heat and Fluid Flow*, **24**, 606–615, (2003).

[25] P. Sweby. High resolution schemes using flux limiters for hyperbolic conservation laws. *SIAM J. Numer. Anal.* **21 (5)**, 995–1011, (1984).

[26] C. M. Rhie and W. L. Chow. Numerical study of the turbulent flow past a airfoil with trailing edge seperation. *AIAA Journal*, **21 (11)**, 1525–1533, (1983).

[27] H. A. Van der Vorst. BI-CGSTAB: A fast and smoothly convecting variant of BI-CG for the solution of nonsymmetric linear systems. *SIAM J. Sci. Stat. Compt.*, **13 (2)**, 631–644, (1992).

[28] J. A. Meijerink and H. A. Van der Vorst. Guidelines for the usage of incomplete decompositions in solving sets of linear equations as they occur in practical problems. *Journal of Cmputational Physics*, **44**, 134–155, (1981).

[29] D. S. Kershaw. The complete Cholesky-conjugate gradient method for the iterative solution of systems of linear equations. *Journal of Cmputational Physics*, **26**, 43–65, (1978).

[30] H. Choi and P. Moin. Effects of the computational time step on the numerical solutions of the turbulent flow. *Journal of Cmputational Physics*, **113**, 1–4, (1994).